LETTER

doi:10.1038/nature11822

Northern Hemisphere forcing of Southern Hemisphere climate during the last deglaciation

Feng He[1], Jeremy D. Shakun[2], Peter U. Clark[3], Anders E. Carlson[1,3,4], Zhengyu Liu[1,5], Bette L. Otto-Bliesner[6] & John E. Kutzbach[1]

According to the Milankovitch theory, changes in summer insolation in the high-latitude Northern Hemisphere caused glacial cycles through their impact on ice-sheet mass balance[1]. Statistical analyses of long climate records supported this theory, but they also posed a substantial challenge by showing that changes in Southern Hemisphere climate were in phase with or led those in the north[2]. Although an orbitally forced Northern Hemisphere signal may have been transmitted to the Southern Hemisphere[3], insolation forcing can also directly influence local Southern Hemisphere climate, potentially intensified by sea-ice feedback[4–6], suggesting that the hemispheres may have responded independently to different aspects of orbital forcing. Signal processing of climate records cannot distinguish between these conditions, however, because the proposed insolation forcings share essentially identical variability[7]. Here we use transient simulations with a coupled atmosphere–ocean general circulation model to identify the impacts of forcing from changes in orbits, atmospheric CO_2 concentration, ice sheets and the Atlantic meridional overturning circulation (AMOC) on hemispheric temperatures during the first half of the last deglaciation (22–14.3 kyr BP). Although based on a single model, our transient simulation with only orbital changes supports the Milankovitch theory in showing that the last deglaciation was initiated by rising insolation during spring and summer in the mid-latitude to high-latitude Northern Hemisphere and by terrestrial snow–albedo feedback. The simulation with all forcings best reproduces the timing and magnitude of surface temperature evolution in the Southern Hemisphere in deglacial proxy records[8,9]. AMOC changes associated with an orbitally induced retreat of Northern Hemisphere ice sheets[10] is the most plausible explanation for the early Southern Hemisphere deglacial warming and its lead over Northern Hemisphere temperature; the ensuing rise in atmospheric CO_2 concentration provided the critical feedback on global deglaciation[9,11].

To identify the physical mechanisms associated with the onset of the last deglaciation, we conducted four single-forcing transient simulations in addition to a transient simulation with all forcings[12] (hereafter ALL), using the Community Climate System Model version 3 (CCSM3) of the US National Center for Atmospheric Research: ORB (22–14.3 kyr BP), forced only by transient variations of orbital configuration[13] (Figs 1a and 2a, b); GHG (22–14.3 kyr BP), forced only by transient variations of atmospheric greenhouse gas concentrations[14] (Fig. 1a); MOC (19–14.3 kyr BP), forced only by transient variations of meltwater fluxes from the Northern Hemisphere (NH) and Antarctic ice sheets[12] (Fig. 1b, c); and ICE (19–14.3 kyr BP), forced only by quasi-transient variations of ice-sheet orography and extent based on the ICE-5G (VM2) reconstruction[15]. All other forcing factors for each single-forcing simulation were held constant at their Last Glacial Maximum value. See Methods for further details.

For comparison with model results, we constructed Southern Hemisphere (SH) regional proxy temperature stacks from records south of the equatorial region (15–90° S), with four surface air temperature (SAT) records used to construct an Antarctic stack, five sea surface temperature (SST) records for the South Atlantic stack, six SST

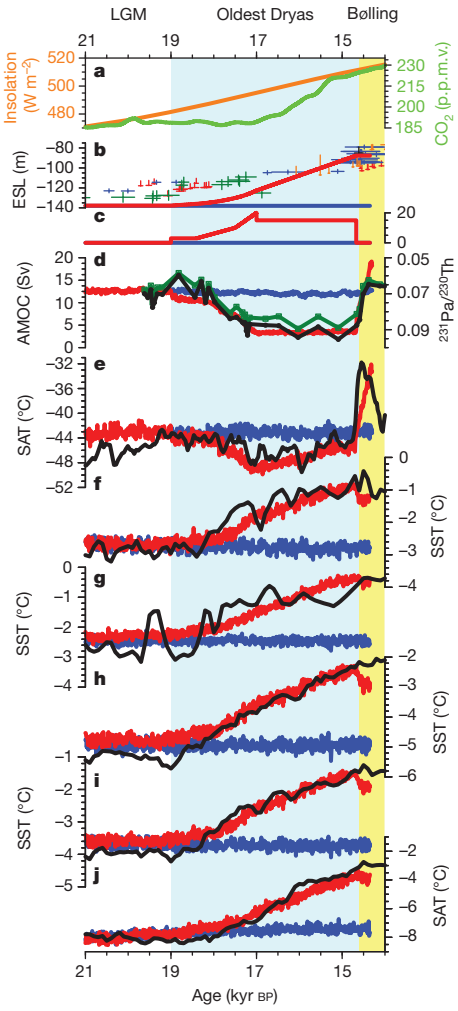

Figure 1 | Comparison of data and models for SH regional temperature stacks. **a**, Insolation on 21 June at 60° N (ref. 13) and atmospheric CO_2 concentration[14]. **b**, Eustatic sea level[28]. Age error bars, ± 2 s.d. **c**, NH meltwater (NHMW) fluxes[12], in metres of global sea level rise per 1,000 years. **d**, Pa/Th ratio at Bermuda (GGC5 core) as a proxy for AMOC export[29], and model maximum AMOC transport (below 500 m). Sv, Sverdrup (1 Sverdrup = 10^6 m^3 s^{-1}). **e**, Greenland SAT based on GISP2 ice core[30] and from simulations (model offset by −4.5 °C). **f**–**i**, Regional SST stack in the South Atlantic (**f**), the Indian Ocean (**g**), the South Pacific (**h**) and the SH Ocean (**i**). **j**, Regional SAT stack over Antarctica. In **d**–**j**: black, reconstruction; red, simulation ALL; blue, simulation ORB (10-year annual averages). LGM, Last Glacial Maximum.

[1]Center for Climatic Research, Nelson Institute for Environmental Studies, University of Wisconsin-Madison, Madison, Wisconsin 53706, USA. [2]Department of Earth and Planetary Sciences, Harvard University, Cambridge, Massachusetts 02138, USA. [3]College of Earth, Ocean, and Atmospheric Sciences, Oregon State University, Corvallis, Oregon 97331, USA. [4]Department of Geoscience, University of Wisconsin-Madison, Madison, Wisconsin 53706, USA. [5]Department of Atmospheric and Oceanic Sciences, University of Wisconsin-Madison, Madison, Wisconsin 53706, USA. [6]Climate and Global Dynamics Division, National Center for Atmospheric Research, Boulder, Colorado 80307, USA.

©2013 Macmillan Publishers Limited. All rights reserved

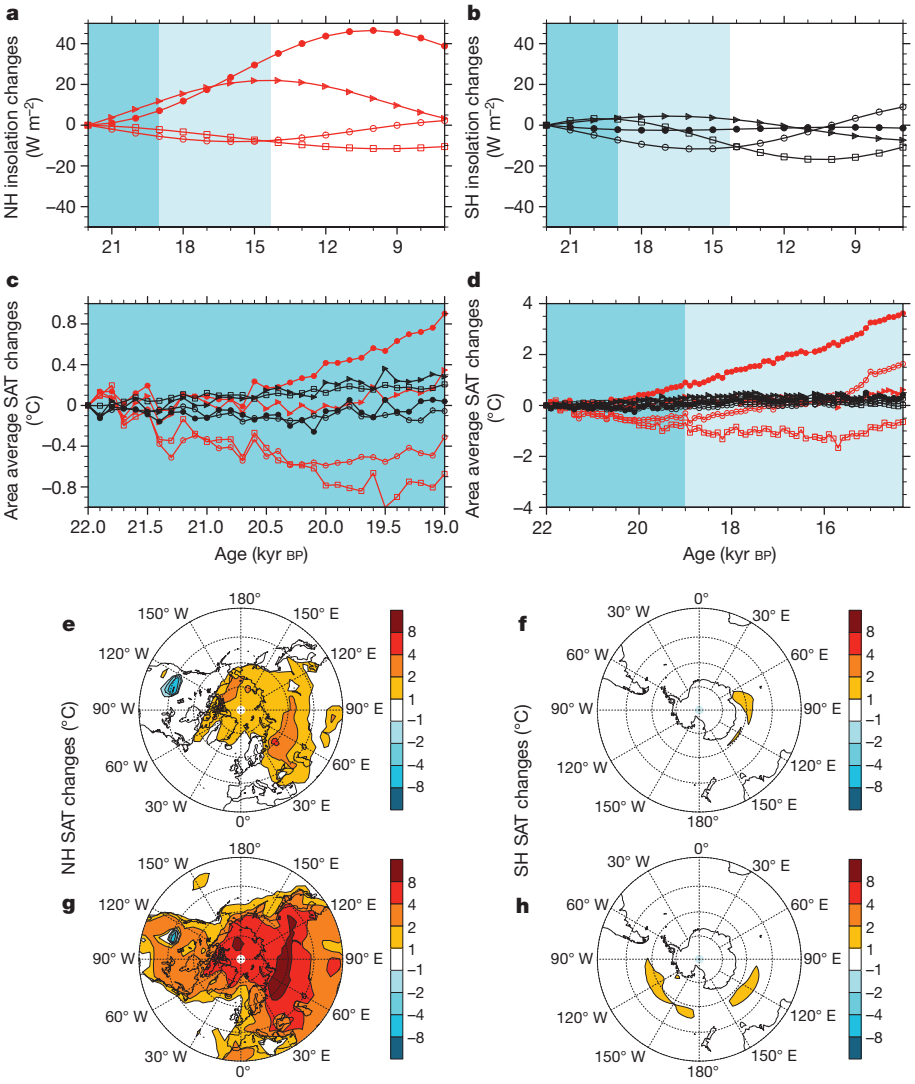

Figure 2 | Comparison of the deglacial warming between the NH and the SH in simulation ORB. **a**, **b**, Insolation changes at the top of the atmosphere in seasonal averages[13]: NH mid–high latitude (40–90° N) (**a**) and SH mid–high latitude (40–90° S) (**b**). **c**, **d**, NH (red) and SH (black) mid–high latitude area average SAT in seasonal averages between 22 and 19 kyr BP (**c**) and between 22 and 14.3 kyr BP (**d**). **e**, **f**, Pattern of SAT changes between 19 and 22 kyr BP in NH summer (June–August) (**e**) and SH autumn (March–May) (**f**). **g**, **h**, Pattern of SAT changes between 22 and 14.3 kyr BP in NH summer (June–August) (**g**) and SH winter (June–August) (**h**). In **a**–**d**: triangles, March–May; filled circles, June–August; open circles, September–November; squares, December–February. The seasons are fixed angular seasons[16,17].

records for the South Pacific stack, two SST records for the Indian Ocean, and the combined 13 SH SST records for the SH SST stack (Supplementary Table 1). The simulated deglacial temperature evolution at the locations of each proxy record is used to derive the corresponding regional deglacial temperature stacks for each transient CCSM3 simulation, providing a direct data-model comparison (Supplementary Figs 1–5).

Simulation ALL captures the timing and much of the amplitude of deglacial warming recorded in SH proxy temperature records between the Last Glacial Maximum and the onset of Bølling warming (22–15 kyr BP) (Fig. 1 and Supplementary Figs 6 and 7). Moreover, the deglacial temperature evolution in the proxy and model ALL stacks identifies the SH lead over the NH, with the onset of deglacial warming starting 19–18 kyr BP in the SH, more than 1 kyr earlier than over Greenland (Fig. 1 and Supplementary Fig. 8). The linear summation of the four single-forcing transient simulations (hereafter simulation SUM) also reproduces the temperature changes in simulation ALL (Fig. 3 and Supplementary Fig. 9), suggesting that the transient climatic responses in these regions are linearly proportional to the changes in the four simultaneous forcings in the coupled climate model.

We use the results from the ORB simulation to evaluate the different hypotheses of orbital forcing of climate during the early deglacial period[3–6]. After correcting for the calendar effect[16,17], which is most pronounced in the SH spring season, we find that the apparent deglacial increase of mid-latitude to high-latitude SH spring insolation[4,6] disappears (Supplementary Figs 10 and 11). The initial increase of the mid-latitude to high-latitude NH spring–summer insolation between 22 and 19 kyr BP was about threefold that in the SH (Fig. 2a, b). Furthermore, the decrease in surface albedo from the melting of terrestrial snow cover in the NH results in additional net solar flux absorption in the NH (Supplementary Figs 12–15). Consequently, NH summers in simulation ORB warm by up to 2 °C in the Arctic and by up to 4 °C over Eurasia, with an area average of 0.9 °C warming in mid to high latitudes in the NH (Fig. 2c, e). In contrast, the simulated area-average SH maximum seasonal temperature change (March–May or December–February) from 22–19 kyr BP increases by only 0.3 °C, with limited regional Southern Ocean warming of less than 2 °C (Fig. 2c, f).

The increase in NH spring–summer insolation continued to exceed the increase in SH insolation throughout the Oldest Dryas (19–14.3 kyr BP), and was about tenfold the anomaly in SH autumn

©2013 Macmillan Publishers Limited. All rights reserved

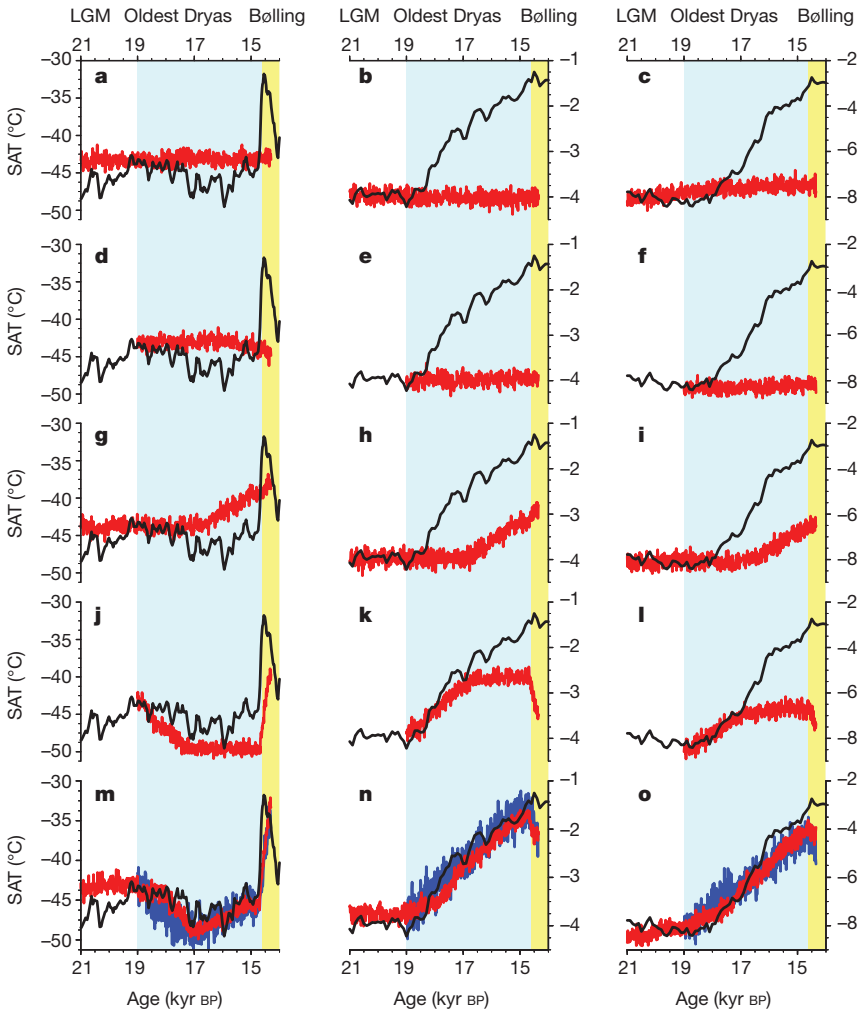

Figure 3 | Early deglacial warming in single-forcing transient simulations. **a**–**c**, Summit Greenland SAT (GISP2) (**a**), SH SST stack (**b**) and Antarctic SAT stack (**c**) in simulation ORB. **d**–**o**, As for **a**–**c**, but for simulations ICE (**d**–**f**), GHG (**g**–**i**), MOC (**j**–**l**) and ALL/SUM (**m**–**o**). All model variables are shown in 10-year annual averages. Proxy reconstructions are shown in black. In **a**–**l**, single-forcing simulations are shown in red. In **m**–**o**, simulation ALL is shown in red, and simulation SUM is shown in blue. LGM, Last Glacial Maximum.

insolation at the end of the Oldest Dryas (Fig. 2a, b). Concurrently, simulated NH summers warm by up to 4 °C in the Arctic and up to 8 °C over Eurasia, mostly due to the snow–albedo feedback (Supplementary Figs 16–19), with an area average of 3.5 °C warming in mid-latitude to high-latitude regions of the NH (Fig. 2d, g). The simulated area-average winter temperature warming in the SH from 22 to 14.3 kyr BP is, however, less than 0.5 °C, with limited regional Southern Ocean warming of less than 2 °C (Fig. 2d, h).

Our ORB simulation thus supports the Milankovitch theory in showing that substantial summer warming occurs in the NH at the end of the Last Glacial Maximum as a result of the larger increase in high-latitude spring–summer insolation in the NH and greater sensitivity of the land-dominated northern high latitudes to insolation forcing from the snow–albedo feedback. This orbitally induced warming probably initiated the retreat of NH ice sheets[10] and helped sustain their retreat during the Oldest Dryas. In contrast, insolation forcing causes significantly less warming in the SH, particularly during the early deglacial period. Most notably, the ORB simulation fails to produce any of the warming seen in the SH regional SST stacks during the Oldest Dryas (Fig. 1). Over Antarctica, the simulated ORB stack shows only ~0.5 °C of deglacial warming, a 90% underestimation of the reconstructed warming in the Antarctic proxy stack (Fig. 1 and Supplementary Figs 9, 20 and 21). Our transient simulations thus suggest that SH orbital forcing alone is too weak to account for the SH warming during the last deglaciation, which can be attributed to the weak response of SH sea ice to the local insolation forcing that was previously suggested to be a strong feedback for amplifying SH orbital changes[4–6] (Supplementary Figs 22–24). An additional shortcoming of hypotheses invoking SH insolation forcing to trigger deglaciation, such as austral spring insolation or summer duration, is that these particular quantities are strong functions of precession and thus cannot readily account for the association between terminations and high obliquity[18].

At the onset of the SH deglacial warming 19–17 kyr BP, simulation ALL reproduces the antiphase annual changes in SAT over Greenland and Antarctica, with 4–6 °C of cooling over Greenland and ~1.5 °C of warming over Antarctica, capturing the timing and much of the reconstructed SH warming (Fig. 3 and Supplementary Figs 25 and 26). In a similar manner to the ORB simulation, the ICE and GHG simulations fail to reproduce significant temperature change in the SH during this interval, as a result of the lack of major changes in ice sheets and concentrations of atmospheric greenhouse gases. In contrast, simulation MOC accounts for almost all of the temperature changes in simulations SUM and ALL (Supplementary Fig. 26), suggesting that the onset of SH warming represents a bipolar seesaw response to the decrease in AMOC associated with the orbitally forced NH ice-sheet retreat that began 20–19 kyr BP[10].

Further support for the role of the bipolar seesaw 19–17 kyr BP comes from the spatial correlation between data and model temperatures from 80 proxy records that span both hemispheres[8,9] (Fig. 4). Among all the single forcing transient simulations, only simulation

©2013 Macmillan Publishers Limited. All rights reserved

MOC shows variability and significant spatial correlation ($P < 0.01$) with the 80 proxy records in terms of the deglacial temperature change during this time, with most of the warming occurring at SH proxy locations and most of the cooling at NH locations (Fig. 4). Simulation MOC also accounts for the significant correlation between the proxy and simulations ALL and SUM during this period (Fig. 4).

The bipolar seesaw 19–17 kyr BP was followed by global warming 17–15 kyr BP from the deglacial increase in CO_2 concentration beginning at ~17.5 kyr BP[9]. Simulation ALL reproduces the in-phase changes among SATs over Greenland and Antarctica and SSTs in the SH (Fig. 3 and Supplementary Figs 27 and 28), whereas simulations ORB and ICE fail to produce significant temperature changes during this interval, because of the cancellation of the seasonal temperature changes from the orbital forcing and the lack of major changes in ice-sheet size. With a weak AMOC 17–15 kyr BP, simulation MOC produces continued but weak warming of SST in the SH and SAT in Antarctica because of thermal inertia in SH oceans during the bipolar seesaw 19–17 kyr BP. Simulation GHG accounts for most of the temperature change in simulations ALL and SUM, suggesting that forcing by greenhouse gases is the dominant mechanism for synchronizing deglacial warming over Greenland and Antarctica and in SSTs in the SH 17–15 kyr BP.

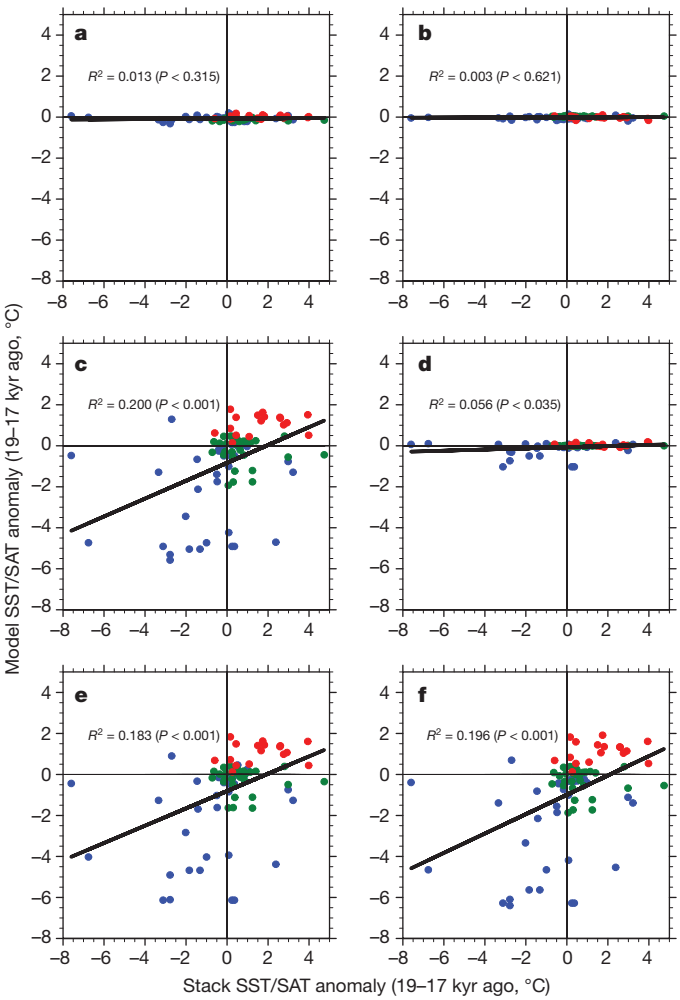

Figure 4 | Spatial correlation of temperature changes of deglacial proxy temperature records[9] and transient simulations between 19 and 17 kyr BP. **a**, ORB; **b**, GHG; **c**, MOC; **d**, ICE; **e**, ALL; **f**, SUM. In the 80 deglacial temperature records, 33 records are from NH mid–high latitude (15–90° N blue), 30 are from the tropics (green) and 17 are from the SH mid–high latitude (15–90° S, red). Temperature changes in the model are based on 300-year annual averages between 17.15–16.85 kyr BP and 19.0–18.7 kyr BP. The solid black line denotes the least-square regression line.

The increase in CO_2 concentration during deglaciations is fundamentally tied to Southern Ocean processes[19] and closely tracks Antarctic temperature changes[20]. The dominance of NH meltwater forcing in triggering SH warming in our model implies that the initial increase in deglacial CO_2 concentration was in turn related to this NH forcing. Moreover, the timing and duration of the steps in the deglacial CO_2 record have been associated with AMOC reductions[21,22], further supporting the importance of NH meltwater in triggering and maintaining the deglacial increase in CO_2 concentration. At the same time, the dominant role of CO_2 in driving deglacial warming in simulation ALL suggests a positive feedback between melting ice sheets and increasing CO_2 concentration[11], with attendant NH meltwater playing the key role in transferring NH deglaciation to the SH and sustaining the deglacial increase in CO_2 concentration. In contrast, the weak response of the Southern Ocean in simulation ORB throughout the first half of the deglaciation suggests that local insolation contributed little to the increase in CO_2 concentration[4,5].

Our results therefore support the Milankovitch theory in identifying a strong NH response to NH insolation forcing. Our results also provide a physical mechanism that can explain the apparent inconsistency between the Milankovitch theory and the early deglacial warming of the SH: the SH lead is caused by the bipolar seesaw (initially induced by NH orbital forcing) that warms the SH and cools the NH[3,23]. The impact of SH orbital variations and simulated sea-ice feedback[4–6] are substantially weaker than the bipolar seesaw and cannot account for the ~1.5 °C warming in the SH regional proxy temperature stacks 19–17 kyr BP. Much of the SH warming during the last deglaciation was therefore driven initially by NH forcing and subsequently by increasing concentrations of atmospheric greenhouse gases. We suggest that our results may apply to each of the major deglaciations of the past 450 kyr. Given the muted Antarctic temperature response to insolation forcing and NH ice-sheet changes simulated in our model, and that Antarctic temperature may consistently lead CO_2 concentration[24,25], NH meltwater forcing associated with large ice sheets provides a viable mechanism for triggering SH deglacial warming and the attendant increase in CO_2 concentration[19], which is consistent with records showing that a decrease in AMOC is a common feature of terminations[21,26,27].

METHODS SUMMARY

We conducted four single-forcing transient simulations of the last deglaciation (ORB, ICE, GHG and MOC) with CCSM3 of the US National Center for Atmospheric Research, to test the impact of these different forcings in the transient simulation ALL[12], and to investigate the contribution of each individual forcing to early deglacial warming in the SH. As in simulation ALL, all single-forcing transient simulations include dynamic vegetation feedback and a fixed annual cycle of aerosol forcing. Similar to simulation ALL, simulations ORB and GHG were branched off from an equilibrium Last Glacial Maximum simulation[12]. Simulation ORB was forced only by transient variations in orbital configuration[13] of the past 22 kyr, and simulation GHG was forced only by transient variations in greenhouse gas concentrations of the past 22 kyr (ref. 14). All other forcing factors for simulations ORB and GHG are held constant with the values of 22 kyr BP. Both simulations MOC and ICE were branched off at 19 kyr BP from simulation ALL. Simulation MOC was forced only by transient variations of NH meltwater fluxes that were identical to those applied in simulation ALL[12]. In simulation ICE, continental ice-sheet orographies and extents were modified on the basis of the time resolution of the ICE-5G (VM2) reconstruction[15]; that is, once per 1,000 years for 19–17 kyr BP, and once per 500 years from 17 kyr BP onwards. All other forcing factors for simulations MOC and ICE are held constant with the values of 19 kyr BP.

The SH regional temperature stacks were derived from the deglacial proxy records[9] that contain most published high-resolution (median resolution 200 years), well-dated (636 radiocarbon dates) temperature records from the last deglaciation; these therefore represent the current state of knowledge on SH deglacial temperature variability. The data were linearly interpolated to 100-year resolution and combined as averages to yield mean temperature time series for the regional temperature stacks.

Received 21 August; accepted 27 November 2012.

1. Milanković, M. *Canon of Insolation and the Ice-age Problem [Kanon der Erdbestrahlung und seine Anwendung auf das Eiszeitenproblem] Belgrade. 1941.* (Israel Program for Scientific Translations, 1969).

©2013 Macmillan Publishers Limited. All rights reserved

2. Hays, J. D., Imbrie, J. & Shackleton, N. J. Variations in Earth's orbit—pacemaker of ice ages. *Science* **194,** 1121–1132 (1976).
3. Imbrie, J. *et al.* On the structure and origin of major glaciation cycles. 1. Linear responses to Milankovitch forcing. *Paleoceanography* **7,** 701–738 (1992).
4. Stott, L., Timmermann, A. & Thunell, R. Southern hemisphere and deep-sea warming led deglacial atmospheric CO_2 rise and tropical warming. *Science* **318,** 435–438 (2007).
5. Huybers, P. & Denton, G. Antarctic temperature at orbital timescales controlled by local summer duration. *Nature Geosci.* **1,** 787–792 (2008).
6. Timmermann, A., Timm, O., Stott, L. & Menviel, L. The roles of CO_2 and orbital forcing in driving Southern Hemispheric temperature variations during the last 21 000 yr. *J. Clim.* **22,** 1626–1640 (2009).
7. Huybers, P. Antarctica's orbital beat. *Science* **325,** 1085–1086 (2009).
8. Shakun, J. D. & Carlson, A. E. A global perspective on Last Glacial Maximum to Holocene climate change. *Quat. Sci. Rev.* **29,** 1801–1816 (2010).
9. Shakun, J. D. *et al.* Global warming preceded by increasing carbon dioxide concentrations during the last deglaciation. *Nature* **484,** 49–54 (2012).
10. Clark, P. U. *et al.* The Last Glacial Maximum. *Science* **325,** 710–714 (2009).
11. Ruddiman, W. F. Ice-driven CO_2 feedback on ice volume. *Clim. Past Discuss.* **2,** 43–55 (2006).
12. Liu, Z. *et al.* Transient simulation of last deglaciation with a new mechanism for Bolling–Allerod warming. *Science* **325,** 310–314 (2009).
13. Berger, A. L. Long-term variations of daily insolation and Quaternary climatic changes. *J. Atmos. Sci.* **35,** 2362–2367 (1978).
14. Joos, F. & Spahni, R. Rates of change in natural and anthropogenic radiative forcing over the past 20,000 years. *Proc. Natl Acad. Sci. USA* **105,** 1425–1430 (2008).
15. Peltier, W. R. Global glacial isostasy and the surface of the ice-age earth: the ICE-5G (VM2) model and GRACE. *Annu. Rev. Earth Planet. Sci.* **32,** 111–149 (2004).
16. Timm, O., Timmermann, A., Abe-Ouchi, A., Saito, F. & Segawa, T. On the definition of seasons in paleoclimate simulations with orbital forcing. *Paleoceanography* **23,** PA2221 (2008).
17. Chen, G. S., Kutzbach, J. E., Gallimore, R. & Liu, Z. Y. Calendar effect on phase study in paleoclimate transient simulation with orbital forcing. *Clim. Dyn.* **37,** 1949–1960 (2011).
18. Huybers, P. & Wunsch, C. Obliquity pacing of the late Pleistocene glacial terminations. *Nature* **434,** 491–494 (2005).
19. Fischer, H. *et al.* The role of Southern Ocean processes in orbital and millennial CO_2 variations—a synthesis. *Quat. Sci. Rev.* **29,** 193–205 (2010).
20. Pedro, J. B., Rasmussen, S. O. & van Ommen, T. D. Tightened constraints on the time-lag between Antarctic temperature and CO_2 during the last deglaciation. *Clim. Past* **8,** 1213–1221 (2012).
21. Cheng, H. *et al.* Ice age terminations. *Science* **326,** 248–252 (2009).
22. Denton, G. H. *et al.* The last glacial termination. *Science* **328,** 1652–1656 (2010).
23. Crowley, T. J. North Atlantic deep water cools the Southern Hemisphere. *Paleoceanography* **7,** 489–497 (1992).
24. Caillon, N. *et al.* Timing of atmospheric CO_2 and Antarctic temperature changes across termination. III. *Science* **299,** 1728–1731 (2003).
25. Hansen, J. *et al.* Climate change and trace gases. *Phil. Trans. R. Soc. A* **365,** 1925–1954 (2007).
26. McManus, J. F., Oppo, D. W. & Cullen, J. L. A 0.5-million-year record of millennial-scale climate variability in the North Atlantic. *Science* **283,** 971–975 (1999).
27. Martrat, B. *et al.* Four climate cycles of recurring deep and surface water destabilizations on the Iberian margin. *Science* **317,** 502–507 (2007).
28. Carlson, A. E. & Clark, P. U. Ice-sheet sources of sea level rise and freshwater discharge during the last deglaciation. *Rev. Geophys.* **50,** RG4007 http://dx.doi.org/10.1029/2011RG000371 (2012).
29. McManus, J. F., Francois, R., Gherardi, J. M., Keigwin, L. D. & Brown-Leger, S. Collapse and rapid resumption of Atlantic meridional circulation linked to deglacial climate changes. *Nature* **428,** 834–837 (2004).
30. Cuffey, K. M. & Clow, G. D. Temperature, accumulation, and ice sheet elevation in central Greenland through the last deglacial transition. *J. Geophys. Res.* **102** (C12) 26383–26396 (1997).

Supplementary Information is available in the online version of the paper.

Acknowledgements We thank O. Timm and A. Timmermann for fruitful discussions, and G. Chen for providing the conversion code for fix-angular calendar. We thank the University Corporation for Atmospheric Research for continuous development of the community Earth system model. This research used resources of the Oak Ridge Leadership Computing Facility, located in the National Center for Computational Sciences at Oak Ridge National Laboratory, which is supported by the Office of Science of the Department of Energy under contract DE-AC05-00OR22725. F.H. is supported by the US National Science Foundation (AGS-0902802, AGS-1203430) and the Climate, People, and the Environment Program. P.U.C. and J.D.S. were supported by the Paleoclimate Program of the National Science Foundation through project PALEOVAR (06023950-ATM). This is CCR contribution no. 1130.

Author Contributions F.H. and Z.L. conceived this study. F.H. initiated and performed all the single-forcing transient simulations and wrote the manuscript with P.U.C. J.D.S. provided and synthesized the proxy data. A.E.C. and P.U.C. constructed the meltwater forcing schemes with F.H., Z.L. and B.O.-B. Z.L. and B.O.-B. initiated the transient simulation project and provided the computational resources. J.E.K. helped interpret the calendar effect of insolation. All authors discussed the results and provided input on the manuscript.

Author Information Reprints and permissions information is available at www.nature.com/reprints. The authors declare no competing financial interests. Readers are welcome to comment on the online version of the paper. Correspondence and requests for materials should be addressed to F.H. (fenghe@wisc.edu).

©2013 Macmillan Publishers Limited. All rights reserved